DØnote xxxx-CONF

The Isolated Photon Cross Section in the Central Rapidity Region at 1.96 TeV.

D. Bandurin

Joint Institute for Nuclear Research, Dubna, Russia

(Dated: May 26, 2005)

A measurement of the inclusive cross section for production of isolated photons is presented for transverse energies in the range of 23−300 GeV for the central region pseudorapidity $|\eta| < 0.9$. The results are based on a data sample of 325.9 pb^{-1} of integrated luminosity accumulated during 2002−2004 in $p\bar{p}$ collisions at $\sqrt{s}$ =1.96 TeV and recorded with the DØ detector at the Fermilab Tevatron Collider. The obtained results are compared with the next-to-leading order QCD predictions using CTEQ6.1M parton distribution functions.

Preliminary Results for Spring 2005 Conferences

I. INTRODUCTION

The production of isolated photons in high energy hadronic collisions has been studied intensively at experiments and theoretically during the last 25 years. In high energy $p\bar{p}$ collisions the dominant source for production of photons with moderate and high transverse momentum p_T is direct (or prompt) photons. They are called direct since they are produced directly from parton-parton interactions and not from the hadron decays (such as π^0, η, K_s^0). These photons come unaltered from the hard process and therefore can give us a clean test of the hard scattering dynamics. In the region up to $p_T^\gamma \simeq 150$ GeV the direct photons are mainly produced through the Compton scattering $q + g \to q + \gamma$ and thus their production cross section is sensitive to the gluon density inside the colliding hadrons. A high center of mass energy at Tevatron and the statistics accumulated currently in Run II allows us to test QCD and gluon distribution in the region of large Q^2 and wide range of $x_{_T}$: $0.02 < x_{_T} < 0.30$. The measurements of isolated photon cross section also allows testing the next-to-leading order (NLO) and resumed QCD calculations, phenomenological models of gluon radiation, studies of photon isolation and the fragmentation process.

Photon identification is free from the uncertainties caused by the parton fragmentation or by experimental issues related to jet identification and energy measurement and thus has an advantage over jet production measurement.

In addition, photons in the final state may be an important sign of new particles and/or physics beyond the standard model. Thus, first of all, it is useful and necessary to study and to understand the "conventional" sources of photons.

This note presents a first measurement of the cross section for production of isolated photons in $p\bar{p}$ collisions at $\sqrt{s}$ =1.96 TeV (Run II) in the central pseudorapidity region of $|\eta| < 0.9$ and covers a much wider p_T^γ range than Run I measurements at CDF [2] and DØ [3]. (Pseudorapidity is defined as $\eta = -ln\ tan\theta/2$, where θ is the polar angle with respect to the proton beam.)

II. ANALYSIS

A. Data sample.

The data used in this analysis were collected during the time period from August 2002 to June 2004 and correspond to a total integrated luminosity 325.9 ± 21.2 pb^{-1}.

B. Selection criteria.

Photon candidates were identified in the DØ detector [4] as isolated clusters of energy depositions in the uranium and liquid-argon sampling calorimeter. The electromagnetic (EM) section of the calorimeter is segmented longitudinally into four layers (EM1-EM4) of 2, 2, 7, and 10 radiation lengths, respectively, and transversely into cells in pseudorapidity and azimuthal angle $\Delta\eta \times \Delta\phi = 0.1 \times 0.1$ (0.05×0.05 in EM3). In addition, the cluster may also contain the energy deposited in the hadronic portion of the calorimeter located after the EM one [4].

To select photon candidates in data and Monte Carlo (MC) we have used the following selections. The data were initially preselected by Common Sample group with requirement of at least one EM objects with $p_T > 15$ GeV. The preselected events are required to pass a combination of the unprescalled EM triggers. The event vertex was required to be within 50 cm of the nominal center of the detector along the beam ($|Z_{vtx}| < 50\ cm$) and should have at least 3 associated tracks.

Each EM object is reconstructed by simple cone algorithm with cone size of $\mathcal{R} = 0.2$. Candidate EM clusters were accepted within region in pseudorapidity $|\eta| < 0.9$. To avoid inter-calorimeter boundaries and cracks EM fiducial cuts are applied. The total geometric acceptance is found to be 0.842 ± 0.002. Each candidate was required to deposit more than 95% of the detected energy in the EM section of the calorimeter (EMfrac > 0.95) and to be isolated in the annular region between $\mathcal{R} = \sqrt{\Delta\eta^2 + \Delta\phi^2} = 0.2$ and $\mathcal{R} = 0.4$ around the gravity center of the cluster: $Iso(\Delta\mathcal{R}02) < 0.10$. Here $Iso(\Delta\mathcal{R}02) = (EisoTot - EisoCore)/EisoCore$, where $EisoTot$ is overall (EM+hadronic) tower energy in (η, ϕ) circle of $\mathcal{R} = 0.4$ and $EisoCore$ is EM tower energy in circle of $\mathcal{R} = 0.2$. Probability to have any track spatially matched to the EM cluster in the event was required to be below 0.001. We also reject events having too large missing E_T by the cut $E_T^{miss}/p_T^\gamma < 0.7$. Photon selection efficiency with respect to these cuts is presented in Fig. 1. It can be fitted by $a - exp[(b - p_T)/c]$ with values of parameters $a = 0.915 \pm 0.004$, $b = -52.04 \pm 6.11$, and $c = 28.43 \pm 1.60$.

A set of additional variables was used for a further background suppression. They are number of cells that belong to the EM cluster, are in EM1, and have a cell energy $E_{cell} > 0.4$ GeV, number of cells with the same E_{cell} threshold and within the ring of $\Delta\mathcal{R} = 0.2 - 0.4$ around the EM cluster, scalar sum of track transverse momenta in the ring of

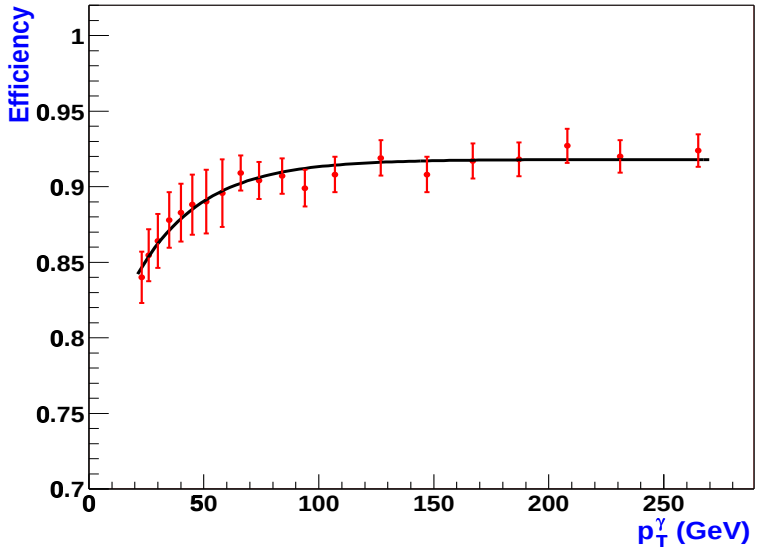

FIG. 1: Photon selection efficiency to pass the main cuts: The events satisfy conditions EMfrac > 0.95, $Iso(\Delta\mathcal{R}02) < 0.10$, no spatially matched tracks and $E_T^{miss}/p_T^\gamma < 0.70$ as a function of p_T. The fitting function is shown on the plot.

$0.05 \leq \mathcal{R} \leq 0.4$ with $p_T^{tr} > 0.3$ GeV, energy weighted EM cluster width in $r \times \phi$ in EM3 layer. These variables have shown consistent behavior on the electrons/positrons from $Z \to e^+e^-$ events.

These variables are new as compared with Run I and they were introduced, on the one hand, to build a discriminant variable that would allow one to determine a photon fraction (purity) in the selected sample and, on the other hand, to specify a criterion for increasing the photon purity.

When discriminating between photons and background particles (π^0 as well as the neutral decay channels of η and K_s^0 mesons) we face a typical (for high energy physics) pattern recognition problem. The standard procedure for solving such a problem is the introduction of relevant cuts in the multi-dimensional data. Nowadays the application of a software-implemented artificial neural network (ANN) for pattern recognition is well known and usually gives the results that are superior to conventional approaches [5].

So, instead of direct application of cuts on these variables they were used to build ANN that can accumulate a power of all the four variables and criteria on them. ANN, based on JETNET package [6], is then applied for an additional selection criterion and following calculation of photon purity. The cut we have applied on the network output is $NN_{output} > 0.5$. A systematic error assigned for this cut is the difference between NN_{output} values for MC and data electrons/positrons from $Z \to e^+e^-$ events and is 2.4% for this cut. Photon efficiency with respect to this cut is turned out to be independent on p_T^γ and agrees with constant 0.937 ± 0.002. The distributions over NN_{output} for direct photon and em-jets and data $44 < p_T^\gamma < 50$ GeV are presented in Fig. 2 with position of the NN_{output} cut.

C. Photon purity estimation.

A measured signal from the isolated photon is contaminated with a background stemming from QCD jets that have fluctuated into the well-isolated single EM cluster. The cluster is caused mainly by energetic (single or multiple) π^0, η, K_s^0 or ω mesons decaying into photons in the final state. These background particles may also be accompanying by soft hadrons whose energy is mostly deposited in the electromagnetic shower developing within the EM cluster.

Since the signal events cannot be identified on an event by event basis their fraction (purity) $\mathcal{P}$ is determined for a given p_T^γ bin statistically. The photon purity is defined as a ratio

$$\mathcal{P} = \frac{N^\gamma}{N^\gamma + N^{jet}} \tag{1}$$

where N^γ (N^{jet}) is the number of single photons (QCD jets) that passed selection criteria.

To determine purity we have used a statistical/probabilistic method. The ANN output in data is fitted by ANN outputs from MC photon and em-jet samples using HMCMLL routine [7] (from HBOOK package). This routine correctly incorporates statistical errors in MC and data histograms and was specially written for fitting MC fractions to data histogram. At high p_T intervals the uncertainty of the found purity points is mostly caused by data statistics while for lower p_T it is mostly caused by the statistics of QCD jets sample which remains after the main selection cuts.

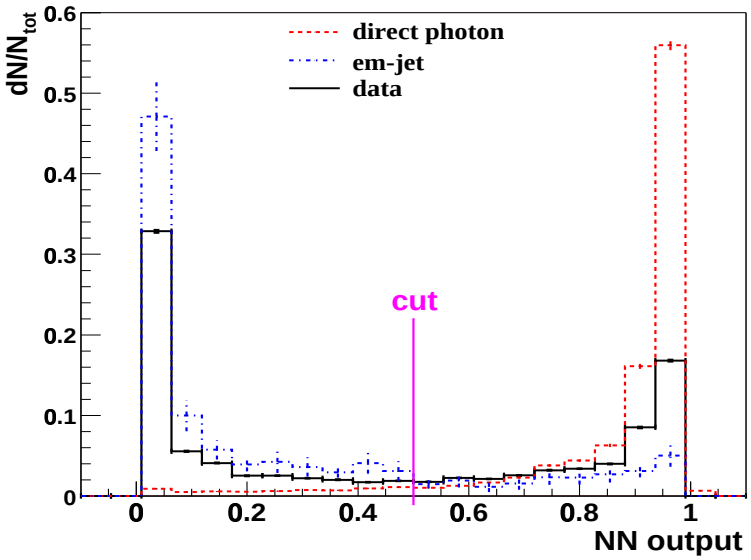

FIG. 2: Normalized distribution of ANN output for data, signal and background events from $44 < p_T^\gamma < 50$ GeV after application of the main selection criteria: EMfrac ≥ 0.95, $Iso(\Delta R02) \leq 0.10$, no spatially matched tracks and $E_T^{miss}/p_T^\gamma < 0.70$. Cut position is shown.

The determined from HMCMLL photon fractions were fitted by function

$$\mathcal{P}_f = 1/(1 + a\ (p_T^\gamma)^b) \tag{2}$$

We have chosen this form because we expect the data to be a sum of two falling cross sections (photons and jets) with their ratio having roughly the form $a(p_T)^b$ (compare with formula (1)). Values of the two free parameters found from fit are $a = 38.86 \pm 16.71$ and $b = -0.971 \pm 0.112$. Besides the main fitting function two other functions can be used: $\mathcal{P}_f = 1 - exp(a + b\ p_T^\gamma)$ and $\mathcal{P}_f = a + b\ ln(p_T^\gamma)$. In Fig.3 we plot the default fit with its statistical error as well as the systematic band in uncertainty caused by usage of alternative fitting functions and by variation of the number of bins in HMCMLL fit. The fit, shown in Fig. 3 with its statistical uncertainty, assures that purity is a smooth function of p_T^γ.

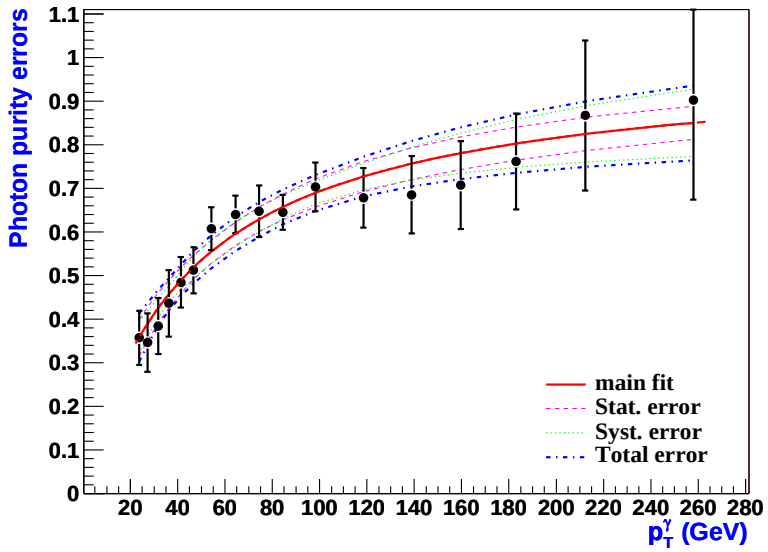

FIG. 3: Default fit (red full line), statistical error from the default fit (purple dashed line), band in systematic uncertainty (green dotted line) and total error (blue dash-dotted line).

An additional systematic uncertainty was assigned due to the fragmentation model used in Monte Carlo event generator PYTHIA [8]. This uncertainty was estimated by varying the ratio between π^0 and η, ω, K_s^0 (containing γ/π^0 in the decay channel) by $\pm 50\%$. Such a variation mostly influences region up to ~ 50 GeV and leads to additional about 7% systematical error in purity at $p_T^\gamma \simeq 25$ GeV, 2% at $p_T^\gamma \simeq 50$ GeV and 1% at $p_T^\gamma \gtrsim 70$ GeV.

D. Photon energy scale and unsmearing corrections.

The calorimeter layer weights used to reconstruct initial energy of the electromagnetic particle were found by using electron based ($Z \to ee, J/\psi \to ee$) events. On the other hand, it is known that photons (due to fundamentally different nature of their interactions) lose noticeably less energy in the material before calorimeter than electrons. This fact can lead to a systematic over-correction in the energy scale for photons and would yield a shift in the cross section. Monte Carlo simulated 'photon+jet' events were used to find necessary corrections. They turned out to be around 1.9% at $p_T^\gamma \simeq$20 GeV, just $\sim$1.0% at 40 GeV and negligibly small at $p_T^\gamma \geq$70 GeV.

Unsmearing is correcting cross section due to finite resolution of the calorimeter. It is especially important for the case of steeply falling spectrum. The unsmearing of p_T^γ spectra was performed with analytical method fitting to the uncorrected cross section a function obtained by the convolution of an initial ansatz (as a physical distribution) and energy resolution function. The correction factors f_{unsm} were then obtained as a ratio of unsmeared (physical) to the smeared fitted function. The found correction can be parametrized by the linear function $f_{unsm} = a - b \cdot p_T^\gamma$ with $a = 0.971 \pm 0.002$ and $b = (9.061 \pm 1.432) \times 10^{-5}$.

III. CALCULATION OF CROSS SECTION AND COMPARISON WITH THEORY.

The inclusive photon cross section was obtained by the relation:

$$\frac{d^2\sigma}{dp_T^\gamma \, d\eta^\gamma} = \frac{N \, \mathcal{P} \, f_{unsm}}{\mathcal{L}_{int} \, \Delta p_T^\gamma \, \Delta\eta^\gamma \, A \, \epsilon_t \, \epsilon_s} \tag{3}$$

where N is number of photon candidates in the selected sample, $\mathcal{P}$ is photon purity, f_{unsm} is unsmearing correction factor, $\mathcal{L}_{int}$ is the integrated luminosity, Δp_T^γ and $\Delta\eta^\gamma$ are the bin sizes in transverse momentum and pseudorapidity, A is the geometric acceptance, ϵ_t is the trigger efficiency, and ϵ_s is the efficiency of selection criteria.

Total number of photon candidates remained after application of all selection criteria is about 2.7 million. They were used to calculate the cross section in 17 p_T^γ bins with average values varied from 23.9 to 258.0 GeV.

The preliminary results of the measurement are shown in Fig. 4 as a function of p_T^γ for the central pseudorapidity region $|\eta^\gamma| < 0.9$ with the full experimental (systematic $\oplus$ statistical) errors. One can see that in the presented range $23.9 < p_T^\gamma < 258.0$ GeV the central photon cross section falls by about 5 orders of magnitude. Statistical errors vary from 0.1% in the first p_T^γ bin to 13.2% in the last bin while systematic errors are within $11 - 25\%$. The largest source of systematic uncertainty is caused by the purity estimation (see Fig.3).

The superimposed theoretical curve corresponds to the QCD NLO predictions based on the code [9, 10] (red full line) with CTEQ6.1M set of parton distribution functions (PDF). The obtained results were also compared with the QCD NLO predictions based on the code [11] with same PDF. The two predictions are based on different sets of fragmentation functions, which are [12] in the first case and [13] in the second. It is worth emphasizing that in spite of such a discrepancy both predictions are in agreement within 7%. A sensitivity of theoretical predictions to the isolation requirements in the ring of $\Delta\mathcal{R} = 0.2$ and to EM fraction in the cone of $\mathcal{R} = 0.2$ was tested [14]. Variation of $Iso(\Delta\mathcal{R}02)$ cut form 10% to 5% and from 10% to 15% leads to changes in cross section $\leq 2\%$. Variation of allowable hadronic energy in the cone of $\mathcal{R} = 0.2$ from 4% to 6% also leads to relative changes in cross section $\leq 2\%$ [14].

The theoretical predictions presented in Fig. 4 correspond to the choice of renormalization, factorization and fragmentation scales as $\mu_R = \mu_F = \mu_f = p_T^\gamma$. If all scales are varied to $\mu_R = \mu_F = \mu_f = 0.5p_T^\gamma$ or to $2p_T^\gamma$ the cross sections are changing within $\pm$12–13% (see Fig. 6).

The ratio of theoretical predictions done with MRST2004 to ones with CTEQ6.1M are shown in Fig. 5. One can see that variations are within 3%.

The ratio of the measured cross section to the NLO QCD predictions [9, 10] calculated with CTEQ6.1M PDF set is presented in Fig. 6. Ratios of the nominal theory predictions [9, 10] (with $\mu_{R,F,f} = p_T^\gamma$ and CTEQ6.1M PDF set corresponding to the best fit) to the predictions with $\mu_{R,F,f} = 0.5p_T^\gamma$ (upper dotted blue curve) and $2p_T^\gamma$ (lower curve) as well as to the predictions with largest upper and lower CTEQ6.1M PDF errors (dash-and-dot red curves) [15] are also shown on the plot. Variation of cross section due to same scale variations obtained with [11] predictions has about the same size ($\pm$1-2%) and p_T^γ dependence.

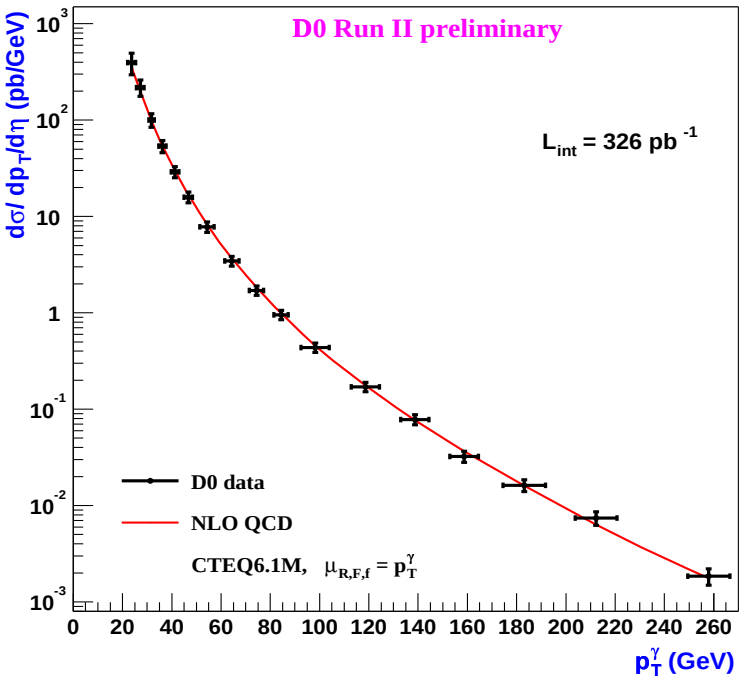

FIG. 4: The inclusive cross section for production of isolated photons $d\sigma/dp_T^\gamma d\eta$ vs. p_T^γ for the central ($|\eta| < 0.9$) pseudorapidity region. The full (systematic $\oplus$ statistical) errors are shown. The red curve is theoretical NLO QCD predictions [9, 10] done for $\mu_R = \mu_F = \mu_f = p_T^\gamma$ with CTEQ6.1M PDF set.

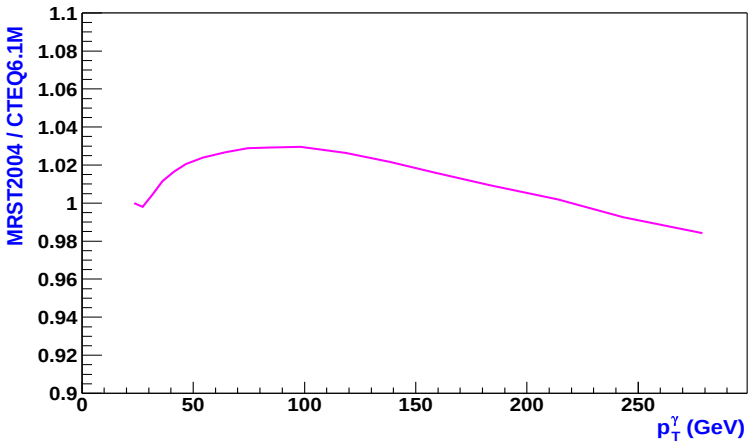

FIG. 5: Ratio of theoretical predictions with MRST2004 to CTEQ6.1M.

From Fig. 6 one can conclude that the theoretical predictions are in agreement with data points within the experimental uncertainties in the whole considered p_T^γ range of $23 \leq p_T^\gamma \leq 300$ GeV.

Acknowledgments

We thank the staffs at Fermilab and collaborating institutions, and acknowledge support from the Department of Energy and National Science Foundation (USA), Commissariat à l'Energie Atomique and CNRS/Institut National de Physique Nucléaire et de Physique des Particules (France), Ministry of Education and Science, Agency for Atomic Energy and RF President Grants Program (Russia), CAPES, CNPq, FAPERJ, FAPESP and FUNDUNESP (Brazil), Departments of Atomic Energy and Science and Technology (India), Colciencias (Colombia), CONACyT (Mexico), KRF (Korea), CONICET and UBACyT (Argentina), The Foundation for Fundamental Research on Matter (The

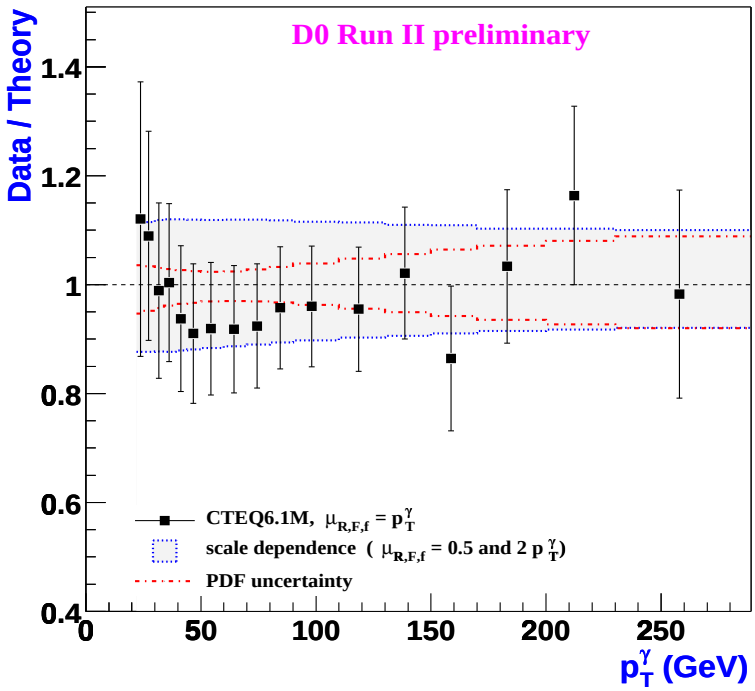

FIG. 6: The ratio of the measured cross section to the NLO QCD predictions done with [9, 10] (theor. predictions based on the code [11] are within 7%), with CTEQ6.1M PDF set is presented. Ratios of the nominal theory predictions (with $\mu_{R,F,f} = p_T^\gamma$ and CTEQ6.1M PDF set corresponding to the best fit) to the predictions with $\mu_{R,F,f} = 0.5 p_T^\gamma$ (upper dotted blue curve) and $2p_T^\gamma$ (lower curve) as well as to the predictions with largest upper and lower CTEQ6.1M PDF errors (dash-and-dot red curves) are also shown on the plot.

Netherlands), PPARC (United Kingdom), Ministry of Education (Czech Republic), Natural Sciences and Engineering Research Council and WestGrid Project (Canada), BMBF (Germany), A.P. Sloan Foundation, Civilian Research and Development Foundation, Research Corporation, Texas Advanced Research Program, and the Alexander von Humboldt Foundation.

[1] E.L. Berger and J. Qiu, Phys.Rev. **D44** (1991)2002.
[2] CDF Collaboration. F. Abe *et al.*, F. Abe *et al.*, Phys.Rev. **D48** (1993)2998; F. Abe *et al.*, Phys.Rev.Lett. **73** (1994)2662;
[3] DØ Collaboration, F. Abachi *et al.*, Phys.Rev.Lett. **77** (1996)5011; DØ Collaboration, B. Abbott *et al.*, Phys.Rev.Lett. **84**(2000)2786; DØ Collaboration, V. Abazov *et al.*, Phys.Rev.Lett. **87**(2001)251805
[4] DØ Collaboration, S. Abachi *et al.*, Nucl.Instrum.Methods, Phys.Res., A**338** (1994)185.
[5] Proc. of CERN School of Computing, 1991, Ystad, Sweden, CERN 92-02, p.113 – 170.
[6] C. Peterson, T. Rognvaldsson and L. Lonnblad, "JETNET 3.0. A versatile Artificial Neural Network Package", Lund University Preprint LU-TP 93-29. Version 3.5 is used here.
[7] R. Barlow, C. Beeston, Comp.Phys.Comm. **77** (1993)219-228.
[8] T. Sjostrand, Comp.Phys.Comm. **82** (1995)74.
[9] P. Aurenche, R. Baier, M. Fontannaz, D. Schiff, Nucl.Phys. **B297** (1988)661; F. Aversa, P. Chiappetta, M. Greco, J.P. Guillet, Nucl.Phys. **B327** (1989)105; S. Catani, M. Fontannaz, J.Ph. Guillet and E. Pilon, Preprint LAPTH-907/02, JHEP 0205 (2002), 028, hep-ph/0204023.
[10] P. Aurenche *et al.*, JETPHOX package, http://wwwlapp.in2p3.fr/lapth/PHOX_FAMILY/main.html. See also [9].
[11] L. E. Gordon and W. Vogelsang, Phys.Rev. **D48**, 3136 (1993); L. E. Gordon and W. Vogelsang, Phys.Rev. **D50**, 1901 (1994).
[12] L. Bourhis, M. Fontannaz, J.P. Guillet, Eur.Phys.J. **C2** (1998)529, hep-ph/9704447.
[13] M. Gluck, E. Reya and A. Vogt, Phys.Rev. **D48**, (1993)116, [Erratum-ibid. D **51**, (1995)1427].
[14] Private (email) communication with W. Vogelsang.
[15] J. Pumplin et al., JHEP 0207, 12 (2002); D. Stump et al., JHEP 0310, 046 (2003).